Applied Catalysis B: Environmental 144 (2014) 233–242

Contents lists available at ScienceDirect

Applied Catalysis B: Environmental

journal homepage: www.elsevier.com/locate/apcatb

On the promoting effect of the addition of ceria to platinum based alumina catalysts for VOCs oxidation

Henri-Joël Sedjame, Céline Fontaine*, Gwendoline Lafaye, Jacques Barbier Jr

IC2MP UMR 7285 CNRS, Université de Poitiers, 4 rue Michel Brunet, 86022 Poitiers Cedex, France

ARTICLE INFO

Article history:
Received 2 May 2013
Received in revised form 3 July 2013
Accepted 8 July 2013
Available online 18 July 2013

Keywords:
Alumina
Ceria
Mixed oxides
n-Butanol
Acetic acid
Oxidation
VOC
OSC

ABSTRACT

Pt catalysts supported on CeO_2–Al_2O_3 mixed oxides with different loadings of ceria (0, 7, 15, 23 and 51 wt%) are prepared by sol–gel method and characterized by S_{BET}, inductively coupled plasma (ICP), hydrogen chemisorption, high resolution transmission electron microscopy (HRTEM), field emission scanning electron microscopy (FESEM), oxygen storage capacity (OSC), X-ray diffraction (XRD) and temperature programmed reduction (TPR). These catalysts are then tested for the complete oxidation of n-butanol and acetic acid. It has been shown that the addition of ceria to alumina influences the physicochemical properties of the materials and their catalytic activities. A decrease of the surface area is observed when adding ceria to alumina. Moreover XRD patterns show that the addition of low concentrations of ceria (7 and 15 wt%) leads to a loss of the alumina structure while the material with a higher ceria loading shows typical crystallized CeO_2 patterns. The reducibility of the materials is enhanced with the increasing ceria loading, which is in accordance with the OSC measurements. Addition of ceria results in the improvement of catalytic performance for n-butanol and acetic acid oxidations even if it also leads to a formation of numerous intermediate products that have mainly been attributed to the actives sites of ceria. A reaction pathway is proposed to explain the formation of these intermediates. The nature of the VOC is found to influence the effect of the addition of ceria on the catalytic activity. In fact, this effect is more pronounced for acetic acid oxidation than n-butanol transformation.

1. Introduction

Nowadays, air pollution is causing serious health problems [1–3]. Therefore, effective techniques for treating those pollutants have been developed. Among those techniques, catalytic oxidation appears to be the most effective for removal of very low concentrations of volatile organic compounds (VOCs) [4]. In fact, catalytic oxidation decreases the temperature of the oxidation compared to thermal methods. The energy consumed is thus lowered. Another advantage of catalytic oxidation in addition to the economic benefit is the reduction of NO_x emissions [5]. Catalytic oxidation requires effective catalysts, depending on some factors such as the nature of the pollutants. In fact chlorinated (CVOC) and sulphur containing (SVOC) organic compounds are known to be more resistant to oxidation than normal VOCs [6]. Hermia and Vigneron have established a correlation between the oxidizability of a VOC and its molar mass; the greater the molar mass, the more difficult is the oxidation [7]. This correlation is in accordance with the order established by Palazzolo and Tichenor regarding the ease of oxidation: alcohols < aldehydes < aromatics < ketones < acetates < alkanes [8].

Noble metal catalysts are often used for the oxidation of various VOCs [9–13], even if they are less resistant to poisons and more expensive than metal oxides [14,15]. According to several authors, among the noble metals, platinum is the most active for VOC oxidation [16–18]. Nevertheless, the catalytic activity of platinum based catalysts depends on the support. Indeed, support properties play an important role in the efficiency of the catalyst. Chuang et al. [19] have showed the influence of the hydrophobic nature of the support for VOC oxidation. Using Pt based-catalysts, they have shown that the oxidation is complete at low temperature when the support used is hydrophobic. Similar results have been obtained by Wu and Wang [20] for toluene oxidation. Papaefthimiou et al. [11] have investigated the influence of acid-base properties of the support for the ethyl acetate oxidation over platinum catalysts. Two supports are used in their work: TiO_2 and TiO_2 (W^{6+}). The most active catalyst is Pt/TiO_2 (W^{6+}), which has a higher density of acid sites.

Ceria is known to have peculiar functions different from other rare-earth oxides [21,22]. It tends to be nonstoichiometric compounds with +4 and +3 oxidation states of cerium atom.

$$CeO_2 \leftrightarrow CeO_{2-y} + \frac{y}{2}O_2 \quad (0 \le y \le 0.5)$$

* Corresponding author. Tel.: +33 549453956.
E-mail address: celine.fontaine@univ-poitiers.fr (C. Fontaine).

0926-3373/$ – see front matter © 2013 Elsevier B.V. All rights reserved.
http://dx.doi.org/10.1016/j.apcatb.2013.07.022

Among these functions, redox properties and oxygen storage capacity (OSC) contribute to improve ceria catalytic properties. In fact, the redox properties of ceria leading to oxygen vacancies and thus to a high oxygen storage capacity helps the thermal resistance of the supports, the dispersion, the oxidation and reduction of supported noble metal and the decrease in coke formation on the catalyst surface [23–27]. The ability of ceria to store and release oxygen makes it an attractive component for mixed oxide catalysts, since it can provide lattice oxygen and prevent the sintering of noble metals. The addition of ceria to another metal oxide such as alumina increases the catalytic activity of the latter [25,28–30]. Ceria plays the role of promoter and reducible support. For example, in the works of Abbasi et al. [28] TPR patterns showed that there was no hydrogen consumption with pure Al_2O_3, while with Al_2O_3–CeO_2 (30 wt%) reduction peaks appeared in the range of 320–1000 °C. In the same work, the promoter effect of addition of ceria to Pt-based alumina catalysts has been proved for the toluene oxidation.

Addition of noble metals to ceria based catalysts is known to increase their rate of reduction and to lead to an obvious improvement of their OSC [25,28,31]. In their work, Ramírez-López et al. [25] showed that the addition of 0.12% of Pd enhanced the reducibility of samples with high ceria loadings (10, 15 and 50 wt%). Similar results are obtained by Abbasi et al. [28] when 1% of Pt has been added to Al_2O_3-CeO_2 (x wt%) supports (x = 10, 20 and 30).

A previous work in our laboratory [32] have demonstrated that Catalytic Wet Air Oxidation (CWAO) of phenol passes through the formation of several organic acids such as maleic acid, acrylic acid and acetic acid. These results are in accordance with the mechanism of phenol oxidation proposed by Delvin and Harris [33]. In this work acetic acid has also been proved to be resistant to the Catalytic Wet Air Oxidation (CWAO). In these experimental conditions (160 and 200 °C), acetic acid is supposed to be found in the gas phase since its boiling point is ~118 °C, hence the need to study the gas phase oxidation. Contrary to CWAO of acetic acid that has been widely studied [34–36], gas phase oxidation of acetic acid is infrequently encountered in the literature. However Ali et al. [37] have proved that among the odorous organic acids, acetic acid is the most difficult to oxidize in gas phase. Using 20 g of a copper catalyst, the complete oxidation of acetic acid has been found to occur at about 250 °C, while the other organics acids (n-Butyric, n-Valeric, i-Butyric and i-Valeric) have been completely destructed at temperatures between 220 and 240 °C.

Even if acid compounds are well known to be difficult to oxidize whereas alcohols are destructed more easily [7,8] the effect of ceria addition can affect differently the oxidation of each of these compounds. Hence, in this paper we will focus on platinum catalysts supported on mixed oxides Al_2O_3–CeO_2 for acetic acid and butanol gas phase oxidation.

In order to investigate the influence of ceria loading on the catalysts activity, Al_2O_3–CeO_2 supports with different loadings of ceria were prepared by sol–gel method. Platinum was impregnated over these materials by incipient wetness impregnation. The preparation method is reported as well as the characterizations of the prepared materials. The complete oxidation of n-butanol and acetic acid has been studied on the catalysts in terms of activity and selectivity. The impact of the nature of the support has then been investigated. A comparison was made between the light off curves of the complete oxidation of n-butanol and acetic acid.

2. Experimental

2.1. Preparation of materials

Five CeO_2–Al_2O_3 mixed oxides and six platinum catalysts were prepared and used for the catalytic tests. These catalysts, the CeO_2–Al_2O_3 supports prepared as well as their abbreviations (AC_x and $PtAC_x$) are listed in Table 1 for sake of clarity. The catalyst PtC_{com} was prepared from commercial ceria support provided by Rhodia.

2.1.1. Preparation of supports

Al_2O_3 and CeO_2–Al_2O_3 supports with different amounts of CeO_2 were prepared by a sol-gel method known as evaporation-induced self-assembly (EISA) method [38]. 5 g of Pluronic P123 were dissolved in 100 mL of ethanol. The solution was stirred at ambient temperature for 1 h. A volume of 6 mL of nitric acid (Aldrich, 90%) and stoichiometrics amounts of aluminum isopropoxide (Aldrich, ≥98%) and cerium acetate (Aldrich, 99.9%) were then added to the solution in order to obtain the expected ceria loading. After stirring for 5 h, the samples were dried in an oven at 60 °C for 5 days. The supports obtained were calcined in a recombined air flow at 400 °C for 4 h (rate 1 °C min^{-1}).

2.1.2. Preparation of Pt-based catalysts

Pt-based catalysts were prepared by incipient wetness impregnation. The supports were impregnated with a Pt salt precursor $Pt(NH_3)_4(OH)_2$. The samples were stirred (250 rpm) overnight and dried at 50 °C for 7 h. The catalysts were calcined at 400 °C under a recombined air flow (60 mL min^{-1}) for 4 h and reduced at 300 °C under a hydrogen flow (60 mL min^{-1}) for 3 h. After reduction, the catalysts were crushed and sieved to obtain particles size lower than 0.25 mm.

2.2. Characterization

2.2.1. Morphological and chemical analysis

The BET specific surface areas were measured by nitrogen physisorption at -195.8 °C using a Micromeritics Tristar apparatus. Samples were previously degassed at 250 °C under high vacuum (0.1–0.2 mbar) overnight. Platinum and ceria loadings were measured by Inductively Coupled Plasma (ICP) using a Perkin–Elmer Optima 2000 DV apparatus. Before analysis, a known mass of powder was dissolved in acid under microwave heating. The metal dispersion was measured by hydrogen chemisorption in a chromatographic microreactor at room temperature for alumina based catalysts and at −85 °C for the catalysts containing ceria to avoid the reduction of the support. Hydrogen pulses (0.25 mL) were injected in regular intervals after reduction under H_2 (300 °C, 1 h).

2.2.2. HRTEM and FESEM analysis

HRTEM measurements were carried out on a Jeol JEM 2100 equipped with a LaB6 filament. The apparatus has a linear resolution of 0.14 nm and is equipped with a Gatan Ultrascan CCD camera with a resolution of 2k × 2k. FESEM measurements were performed on a Jeol JL 5600 LV equipped with a Tungsten filament. Before analysis, powder was dispersed in ethanol, and the solution dropped on a copper grid.

2.2.3. Oxygen storage capacity analysis

The oxygen storage capacity was measured following the oxidation of carbon monoxide in transitory regime without oxygen in gas phase by means of two different techniques (OSC and OSCC). The OSC was measured at 400 °C under atmospheric pressure using a conventional set-up described in a previous work [39]. The sample was continuously purged with helium (30 mL min^{-1}). Successive or alternative pulses (0.265 mL) of O_2 (≤ 5 ppm total impurities) and CO were injected every 2 min [35,40]. The OSC was calculated from the CO consumption after the sample was stabilized in alternates pulses (CO/O_2) [41]. The reaction occurring is the following: $CO_{(g)} + 1/2\ O_{2(s)} \rightarrow CO_{2(g)} + \square_{(s)}$. Such a treatment gives information about both surface and bulk mobile oxygen species. However, under dynamic conditions, surface species are often more involved.

Table 1
Catalysts, abbreviations and morphological data. A stands for Al_2O_3, C for CeO_2.

Supports and catalysts	Abbreviations	Specific surface area ($m^2\,g^{-1}$)	Mean pore size (Å)	Pt loading (wt%)	Ceria loading (wt%)	Dispersion (%)
Pt/CeO_2	PtC_{com}	132	32	0.35	100	14
Al_2O_3	AC_0	196	121	–	0	–
7% CeO_2–Al_2O_3	AC_7	204	113	–	7	–
15% CeO_2–Al_2O_3	AC_{15}	101	92	–	15	–
23% CeO_2–Al_2O_3	AC_{23}	98	86	–	23	–
51% CeO_2–Al_2O_3	AC_{51}	99	63	–	51	–
Pt/Al_2O_3	$PtAC_0$	197	117	0.25	0	80
Pt/7% CeO_2–Al_2O_3	$PtAC_7$	207	110	0.25	7	19
Pt/15% CeO_2–Al_2O_3	$PtAC_{15}$	95	85	0.25	15	48
Pt/23% CeO_2–Al_2O_3	$PtAC_{23}$	95	87	0.25	23	45
Pt/51% CeO_2–Al_2O_3	$PtAC_{51}$	95	62	0.2	51	31

Therefore, OSC experiments were also carried out by re-oxidizing the samples with O_2 pulses. Then alternating pulses of CO and O_2 were injected to probe the amount of O_2 immediately available in these materials, which is supposed to be mainly involved in the catalytic process. Results were collected by a gas phase chromatograph equipped with a TCD detector and a Porapak Q column.

2.2.4. X-Ray analysis

Diffractograms and crystallite size were determined by XRD experiments using a PANalytical Empyrean θ-θ diffractometer using a CuKα radiation ($\lambda_{K\alpha}$ = 1.54186 Å) and equipped with a linear detector Xcelerator. The XRD patterns were obtained under the following conditions: dwell time, 180 s, step 0.05°, constant divergence slit 0.5°. The average crystallite size (d) was calculated using Scherrer's equation: $d = K\lambda_{K\alpha}/\beta_c \cos\theta$ with $\beta_c = (\beta^2 - \beta_0{}^2)^{1/2}$, where β (in rad) is the half-maximum line breath of the analyzed material, β_0 (in rad) is the half-maximum line breath of a perfectly well-crystallized LaB_6 standard, K = 0.9 and θ is the Bragg angle for the diffraction peak considered.

2.2.5. Temperature programmed reduction (TPR)

Prior to the TPR, the catalysts were first pretreated in situ under O_2 for 30 min at 400 °C, and cooled down to 100 °C. The TPR experiments were performed with a 1.0 vol% H_2/Ar gas mixture. The temperature range was 100–900 °C with a ramp of 5 °C min^{-1} and then maintained at 900 °C for 1 h. The measurements of the H_2 consumption were made in an AutoChem II/Micromeritics apparatus, using a thermal conductivity detector.

2.3. Catalytic tests

The gaseous feed used for the catalytic tests was composed of 1000 ppm of VOC in synthetic air. VOC and water were heated in two thermostated saturators. Nitrogen was bubbled through these saturators and the outflow was mixed with the synthetic air. At the reactor inlet the gas stream was composed of 19.38% of O_2, 77.52% of N_2, 3% of H_2O and 0.1% of VOC. Transfer lines were heated at 110 °C to avoid any condensation. The total flow rate was kept constant for all experiments (70 mL min^{-1}). Reactions were carried out in a tubular fixed bed reactor placed in an electrical furnace equipped with a temperature programmer. A thermocouple was inserted inside the catalytic bed to measure exactly the reaction temperature. A mass of 140 mg of catalyst mixed with 1 g of cordierite were used for the reactions. The space velocity was 60,000 h^{-1}. The reaction products were analyzed by a gas chromatograph (Varian 490-GC) equipped with a thermal conductivity detector (TCD) and two columns: a Porapak Q (PPQ) to analyze air and carbon dioxide and a CP sil-5CB to analyze hydrocarbons (butanol, butanal, acetic acid...). Experiments were performed between 50 and 350 °C and the temperature was increased linearly by 0.5 °C min^{-1}. The uncertainty on the results is about ±1 °C. It is important to note that a VOC adsorption is observed when the catalytic test begins: the VOC amount at the reactor outlet increases slowly until it reaches 1000 ppm or slightly exceeds this value if a desorption occurs at the same time. In the case of n-butanol, the conversion curves presented in this paper begin while the adsorption is still occurring, because the n-butanol decomposition starts early. The adsorption is no longer visible between 80 and 90 °C for all catalysts. In the case of acetic acid, the conversion plots presented in this paper begin when adsorption is no longer visible and the quantity of VOC at the reactor outlet is higher than or equal to 1000 ppm. The light off curves exceed sometimes 100% because of a phenomenon of adsorption-desorption occurring during the reaction.

3. Results and discussion

3.1. Characterization

3.1.1. Morphology measurements

The morphological data for all the catalysts prepared are summarized in Table 1. The specific surface area of the catalyst prepared with commercial support PtC_{com} is 132 $m^2\,g^{-1}$. $PtAC_0$ has a specific surface area similar to the catalysts with 7 wt% of ceria. $PtAC_7$ has the higher surface area (~207 $m^2\,g^{-1}$), whereas the addition of 15, 23 and 51 wt% of ceria to the alumina support prepared by sol–gel method decreases by more than half the specific surface area. The reduction of the specific surface area by the addition of ceria has already been observed in the literature [25,28]. These authors agree that this loss of surface area is due to a covering of the alumina surface by ceria. An alumina pore plugging by ceria crystals has also be proposed to explain the decrease of surface area [25]. The decrease of the mean pore size with increasing the ceria loading observed in Table 1 confirms the hypothesis of alumina pore plugging proposed to explain the loss of surface area. In fact it can be seen that the addition of 51 wt% of ceria approximately halved the mean pore size of $PtAC_0$.

The increase of the metal dispersion observed with increasing the ceria loading explained in the literature by the fact that the interaction between Pt and CeO_2 helps to maintain the metal in an oxidized state which avoids the sintering [42] is not observed in this work because $PtAC_0$ has already a very good dispersion. Nevertheless, Damyanova et al. have reported that the oxidation state of platinum increases with the increasing ceria loading, which leads to a decrease in Pt sintering [23]. Moreover, the use of base-metal oxides additives such as CeO_2 has already been proposed by Yermakov and Kuznetsov to increase the dispersion of noble metal on γ-Al_2O_3 [43].

3.1.2. HRTEM and FESEM analysis

Fig. 1(a) and (b) show the FESEM images of AC_7 and AC_{23} respectively. The mapping of aluminum and cerium (Fig. 1(c) and (d)

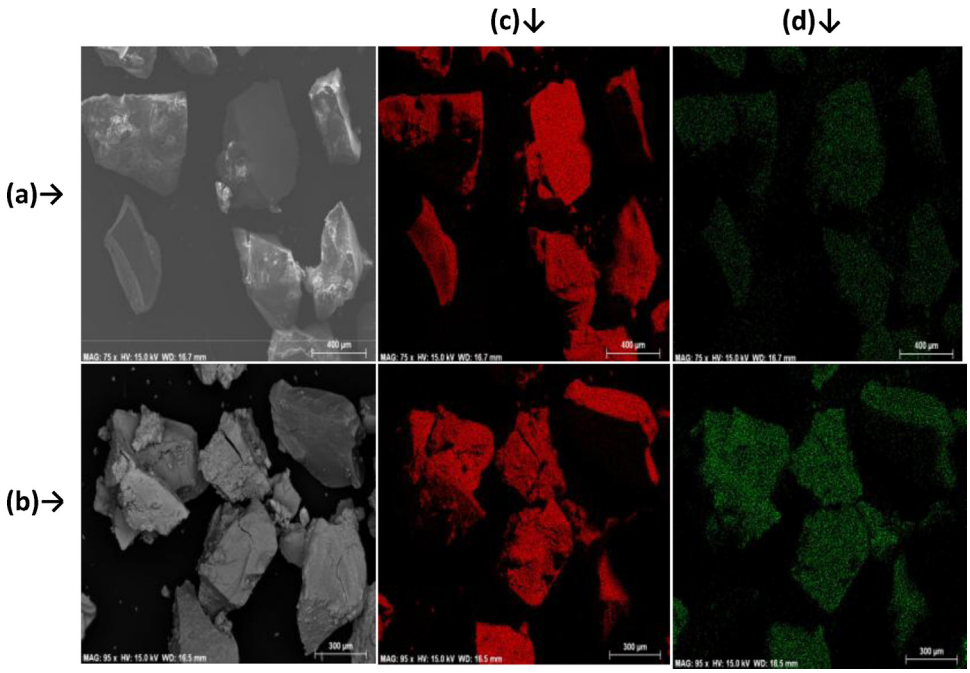

Fig. 1. FESEM images of (a) AC7 and (b) AC23 with a mapping of (c) aluminum and (d) cerium.

respectively) shows the presence of these compounds into the particles of the mixed oxide material. As expected, a comparison between the mappings of cerium on both supports (fig. 1(d)) shows that the density of cerium is more intense in AC_{23} than in AC_7. However the intensity of aluminum density is the same for both materials (Fig. 1(c)).

The morphology and microstructure of synthesized supports has been investigated by TEM technique. Fig. 2 shows the HRTEM images of AC_0 (a), AC_7 (b), AC_{15} (c), AC_{23} (d) and AC_{51} (e) as well as the EDS patterns of an enlarged HRTEM image of AC_{23}. The EDS micro analyses confirm the presence of ceria on the surface of alumina for all Al_2O_3–CeO_2 materials. No crystallized ceria particles have been noticed for AC_7 and AC_{15} while on the supports containing the highest proportions of ceria (AC_{23} and AC_{51}), agglomerates of small particles of crystallized ceria can be observed. The size of these particles is about 2 nm (Fig. 2).

3.1.3. XRD measurements

XRD diffraction patterns of the different supports are reported in Fig. 3A. The patterns for synthesized supports AC_0, AC_7, AC_{15}, AC_{23} and AC_{51} are illustrated in Fig. 3A(a)–(e) respectively. AC_0 shows typical crystallized γ-alumina patterns well defined in region of 2θ values = 19.5°, 32.5°, 37°, 39°, 45.3°, 61°, 66.9° and 85°, as displayed in Fig. 3A(a).

The samples with ceria loadings lower than 23 wt% exhibit amorphous phases (Fig. 3A(b) and (c)). Crystallized ceria is observed for the supports with the highest ceria loadings (23 and 51 wt%). In fact, in Fig. 3A(d) and (e), the crystallized ceria is indicated by diffraction peaks at 2θ = 28.8°, 32.96°, 48.86°, 56.56°, 58.46° and 77.61° corresponding to the reticular planes of CeO_2. The crystallite size for these samples calculated using the Scherrer equation is about 2.2 mm in accordance with the HRTEM analysis (Fig. 2).

After re-calcination which was realized after Pt impregnation, crystallized ceria is observed for the material containing 15 wt% of ceria (Fig. 3B) while $PtAC_7$ catalyst remains in amorphous phase.

3.1.4. Temperature programmed reduction (TPR)

Fig. 4 shows the hydrogen uptakes as a function of temperature, obtained for the calcined CeO_2–Al_2O_3 carriers and Pt/CeO_2–Al_2O_3 catalysts. TPR profiles for unsupported CeO_2–Al_2O_3 carriers exhibit a broad peak in temperature region from 350 to 700 °C (Fig. 4(a)–(d)). This result is similar to those obtained by Ramirez et al. [25]. According to the literature this peak can be attributed to the reduction of superficial cerium oxide [23,28,44]. The reduction of CeO_2 bulk to Ce_2O_3 is known to occur at temperatures higher than 900 °C [23,28]. The maximum and the intensity of the reduction peak increase with the increasing ceria loading. Thus the reduction peaks of the supports with 7 and 15 wt% of ceria occur at 490 and 515 °C respectively, which is expected. In fact the greater the content of ceria, the greater should be the H_2 consumption. The TPR profile of $PtAC_{51}$ shows a small peak at around 351 °C overlapped with the broad peak which maximum is around 553 °C, the hydrogen consumption starts earlier on this catalyst. At 650 °C, the sample with 23 wt% of ceria shows a shoulder overlapped with a broad peak which maximum is around 534 °C.

The addition of platinum strongly lowers the temperature range of hydrogen consumption (110–430 °C). Otherwise, the presence of platinum facilitates the reduction of ceria. This result is in accordance with the literature [45] and it is generally explained by the hydrogen spillover effect due to the metallic platinum. The peak attributed to the reduction of ceria's superficial oxygen reaches a maximum at 285 °C for the catalysts with 7 wt% of ceria (Fig. 4(e)). This maximum shifts to a higher temperature (≥317 °C) for the catalysts with a ceria loading higher than 15 wt% of ceria. The platinum catalysts with 23 and 51 wt% of ceria exhibit a broad peak overlapped with a shoulder at lower temperature (295 °C) that can be attributed to the reduction of the oxidized platinum species. At temperatures higher than 700 °C the TPR profiles of the platinum catalysts exhibit a peak corresponding to the reduction of the CeO_2 bulk. This peak reaches its maximum at around 790, 822 and 866 °C for the platinum catalysts with 7, 15 and 23 wt% of CeO_2 respectively (Fig. 4(e)–(g)). For the $PtAC_{51}$ catalyst the reduction of ceria bulk occurs probably at temperatures higher than 900 °C.

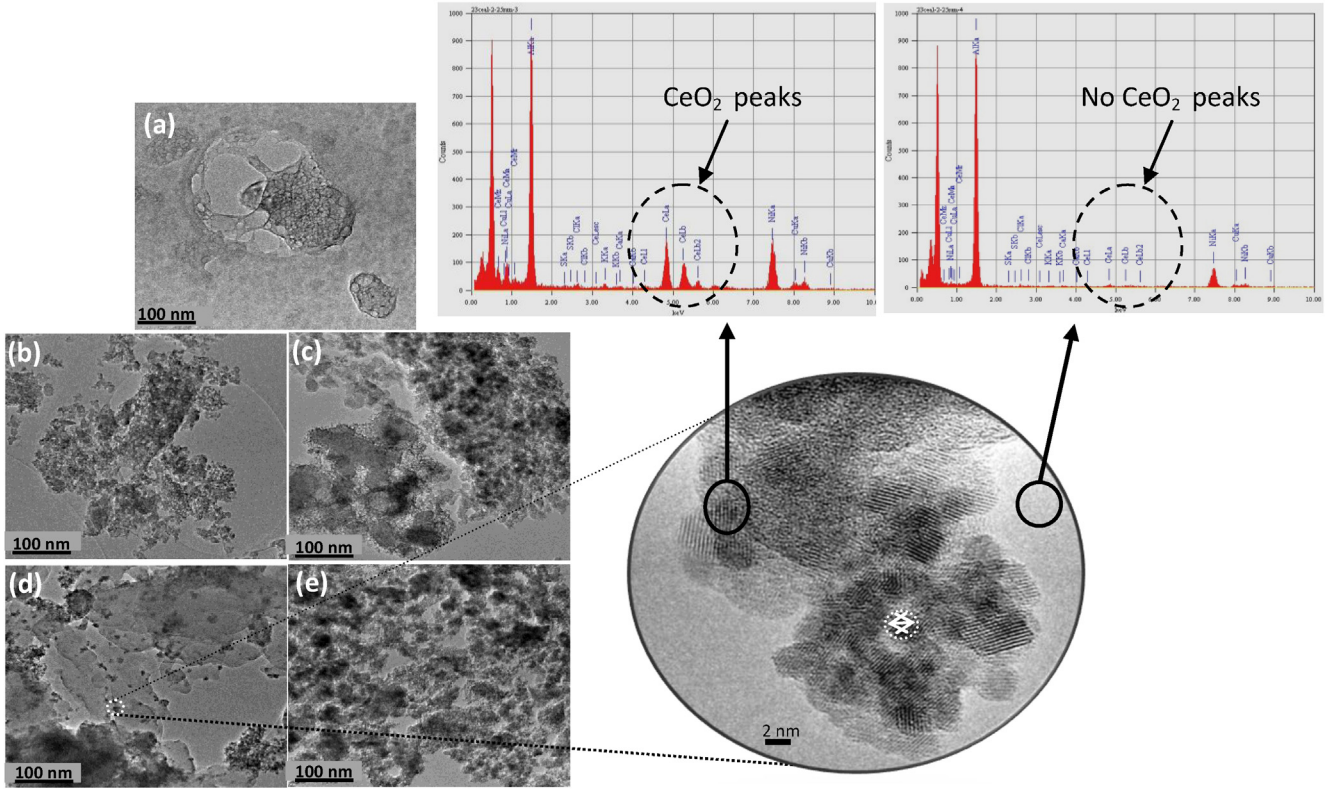

Fig. 2. HRTEM images of the synthesized supports: (a) AC_0, (b) AC_7, (c) AC_{15}, (d) AC_{23} and (e) AC_{51} and EDS patterns of AC_{23}.

3.1.5. Oxygen storage capacity

The oxygen storage capacity was determined at 400 °C in order to calculate the amount of oxygen available from the material during its reduction by CO. CO is thus oxidized into CO_2. Fig. 5 shows the diagrams of oxygen storage capacity values as a function of ceria content for the supports and the platinum based catalysts. Considering that the reduction of oxidized Pt species ($Pt^{x+} \rightarrow Pt^0$) is known to occur at temperatures lower than 400 °C [28], the contribution of this reduction is evaluated to be between 10 and 18 μmol O g^{-1}. Therefore, the OSC values for platinum catalysts containing ceria were calculated by subtracting the contribution of the reduction of platinum.

As expected, the OSC values increase with the ceria loading on the supports with an optimum for 51 wt% of ceria. Thus with an addition of 23 wt% of ceria the amount of oxygen removed by the material raises from 0 to 78 μmol O g^{-1}. This result shows that the addition of ceria to alumina has a promoting effect on the reducibility of the material. The addition of a small amount of platinum enhances significantly the oxygen storage capacity. For example, the OSC of the support containing 23 wt% of ceria increases from 78 to 434 μmol O g^{-1} when platinum is added. This enhancement could be attributed to the fact that CO can adsorb on the metal and by a spillover process it could react at the CeO_2–Al_2O_3 interface. It can also be pointed out that the OSC value of the support with 51 wt% of ceria is higher than that of bare ceria as the OSC values of platinum catalysts with 23 and 51 wt% of ceria are higher than that of the platinum catalyst containing 100 wt% of ceria. Such results have been already obtained for several ceria mixed oxide such as CeO_2–Al_2O_3 [38,46] and CeO_2–ZrO_2 [41]. The presence of small ceria crystallites, as shown by TEM and XRD, as well as the defective structure due to the presence of aluminum atoms into the ceria structure or vice versa may explain the high reducibility of these materials. The increase of oxygen storage capacity observed with ceria loading could suggest an improvement of the catalytic activity as provided in the literature [23–27].

3.2. Catalytic tests

3.2.1. N-butanol oxidation

N-butanol complete oxidation is known to pass through butanal formation following the reaction: n-butanol → butanal → CO_2 [9].

Fig. 6 presents the plots of butanal and carbon dioxide formation ((a) and (b) respectively) as function of temperature for the platinum catalysts and for the supports AC_0 and AC_7. At the beginning of the experiments an adsorption of n-butanol over the catalysts is observed. This adsorption is more or less important depending on the catalyst and is compensated by a desorption occurring at higher temperatures (desorption corresponding to a product yield higher than 100% as shown in Fig. 6). Table 2 lists T_{50} and T_{90} values (temperatures required to obtain a VOC conversion equal to 50 and 90% respectively) as well as selectivity to CO_2 at these temperatures for n-butanol complete oxidation. It is important to note that the higher the T_{50} or the T_{90}, the lower is the catalytic activity. In

Table 2
T_{50}, T_{90} and selectivity to CO_2 values of platinum catalysts used for n-butanol oxidation.

Catalysts	n-Butanol oxidation		Selectivity to CO_2 (%)	
	T_{50} (°C)	T_{90} (°C)	at T_{50}	at T_{90}
PtC_{com}	106	135	7	22
AC_0	152	188	6	19
AC_7	161	189	28	39
$PtAC_0$	143	165	9	27
$PtAC_7$	158	174	29	42
$PtAC_{15}$	157	172	30	42
$PtAC_{23}$	138	167	14	41

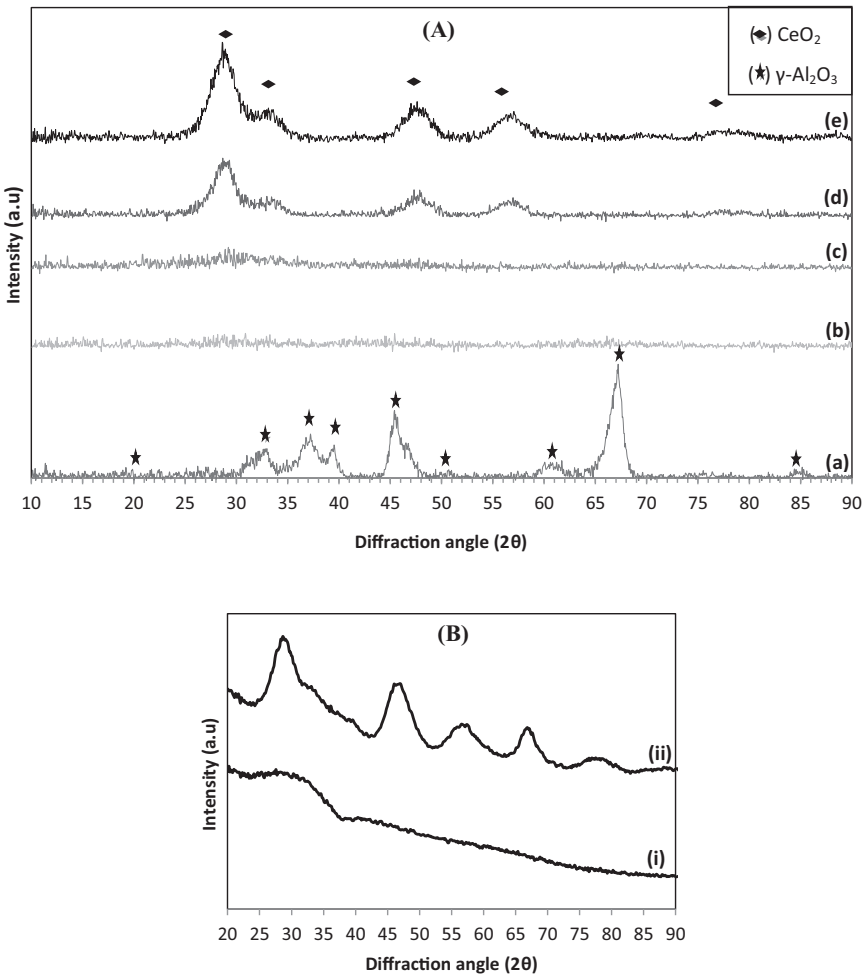

Fig. 3. XRD diffraction patterns of: (A) synthesized supports ((a) AC_0, (b) AC_7, (c) AC_{15}, (d) AC_{23} and (e) AC_{51}) and (B) the materials with 15 wt% of ceria ((i) AC_{15} and (ii) $PtAC_{15}$).

all cases, n-butanol is completely destructed at temperatures lower than 250 °C.

Platinum catalyst supported on commercial support appears to be the most effective for n-butanol total oxidation (Table 2). For this catalyst T_{50} and T_{90} are the lowest. The temperature required to obtain the same conversion with the others platinum catalysts is increased by more than 30 °C for a conversion of 50% and more than 15 °C for a conversion of 90%. This result could be due to the higher platinum content of this catalyst (Table 1).

On PtC_{com}, butanal forms more slowly and reaches its maximum at ~130 °C (Fig. 6(a)). At these temperatures, the formation of carbon dioxide is just beginning, which explains the low selectivity to CO_2 at T_{50} for this catalyst (Table 2). On this catalyst butanal disappears completely at ~165 °C (Fig. 7(a)). The mixed oxide with 7 wt% of ceria (AC_7) exhibits a lower activity for n-butanol complete oxidation than the pure alumina prepared by a sol–gel method (AC_0) at low temperatures. As shown in Table 2, the temperature required to obtain 50% of n-butanol conversion is increased by 9 °C (from 152 °C for AC_0 to 161 °C for AC_7). At higher temperatures both carriers exhibit the same activity for n-butanol complete oxidation (Table 2). Nevertheless, it is important to point out that, at the same conversion, AC_7 presents a higher selectivity to CO_2 (28% vs 6% for AC_0) as shown in Table 2. Moreover Fig. 6 shows that with AC_7, butanal transformation and carbon dioxide formation occur at lower temperatures. Actually, butanal is completely converted at 228 °C with AC_7 whereas it totally disappears at around 240 °C with AC_0 (Fig. 6(a)). Similarly, at 250 °C the CO_2 yield reaches 100% with AC_7 while it is 85% with AC_0 (Fig. 6(b)).

Addition of platinum to these carriers promotes n-butanol complete oxidation (Table 2) and the formation of butanal and CO_2 (Fig. 6). The promotion of n-butanol complete oxidation is more pronounced at higher temperatures as shown in Table 2. Actually, by adding platinum, the T_{50} values are lowered by 9 and 3 °C for AC_0 and AC_7 respectively whereas the T_{90} values are lowered by 23 and 15 °C for AC_0 and AC_7 respectively (Table 2). The catalytic activity of pure alumina seems to be more influenced by the addition of platinum. Fig. 6(a) shows that in the presence of platinum, the temperatures of appearance and total disappearance of butanal decrease by about 45 °C. Similarly, the temperature required to obtain a CO_2 yield of 50% is lowered by more than 25 °C in presence of platinum (Fig. 6(b)). Actually such promoting effect of platinum is well known for VOC oxidation [11].

The platinum catalyst with 15 wt% of ceria ($PtAC_{15}$) presents an activity similar to that of $PtAC_7$ for n-butanol complete oxidation, while $PtAC_{23}$ exhibits an activity similar to that of $PtAC_0$ at higher temperatures (Table 2). In all cases, for these platinum catalysts, in presence of ceria, the selectivity to CO_2 is higher (for the same conversions of n-butanol) (Table 2). Fig. 6(a) shows that in the presence of ceria, butanal is formed in lower amount. This result can be explained by the fact that in presence of ceria several intermediates products others than butanal are formed. These intermediates products, detected by gas chromatography, are

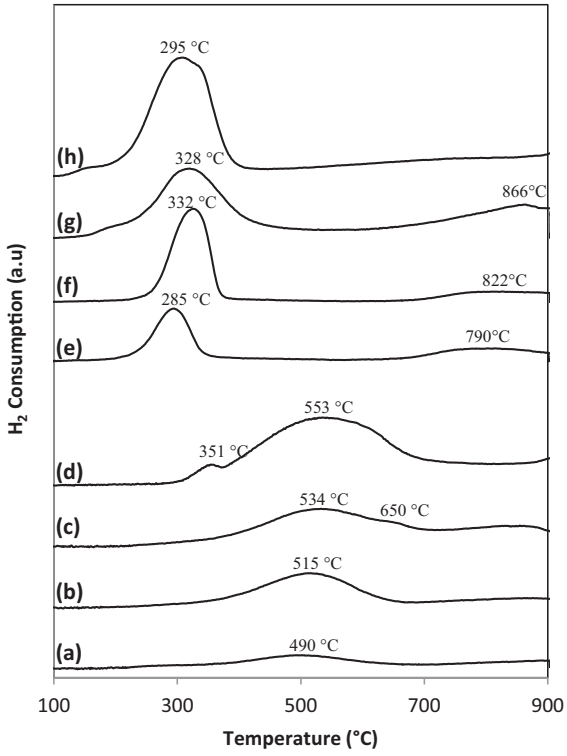

Fig. 4. TPR patterns of calcined: (a) AC_7, (b) AC_{15}, (c) AC_{23}, (d) AC_{51}, (e) $PtAC_7$, (f) $PtAC_{15}$, (g) $PtAC_{23}$ and (h) $PtAC_{51}$.

found to be formaldehyde, methanol, ethanol, acetone (propanol, isopropanol and propanal peaks are combined to that of acetone) and acetic acid. Fig. 7 shows the selectivity to these intermediate products and to CO_2 for all the catalysts. Methanol and acetone are the only intermediates products (others than butanal) observed with the platinum catalysts supported on pure alumina. They are formed in very small quantity. With PtC_{com} the total selectivity to these intermediate products is lower than with the platinum catalysts supported on CeO_2–Al_2O_3. At 250 °C all the by-products are converted into carbon dioxide.

In order to investigate the role of the noble metal and the support in the formation of the intermediates products others than butanal, the selectivity to these products is presented in Fig. 7(c) and (d) for the carriers AC_0 and AC_7 and for the corresponding platinum catalysts. It appears that the same intermediates are formed with AC_7 in almost the same proportion with $PtAC_7$. However with AC_0 and $PtAC_0$ these intermediates are formed in very small quantity. Therefore, the formation of these intermediates products could be attributed mainly to the actives sites of ceria.

A reaction pathway is then proposed for the formation of all the intermediates products over ceria based catalysts (Fig. 8).

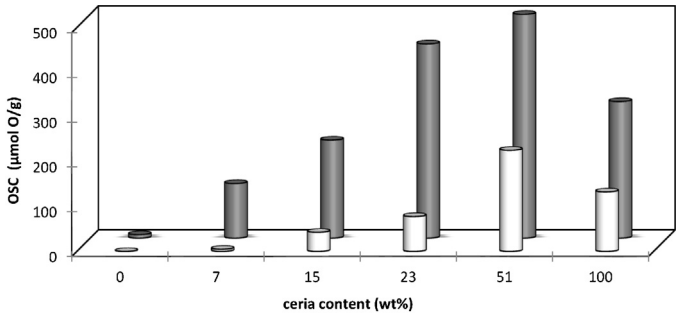

Fig. 5. Oxygen storage capacity of AC_x (□) and $PtAC_x$ (■) versus ceria content.

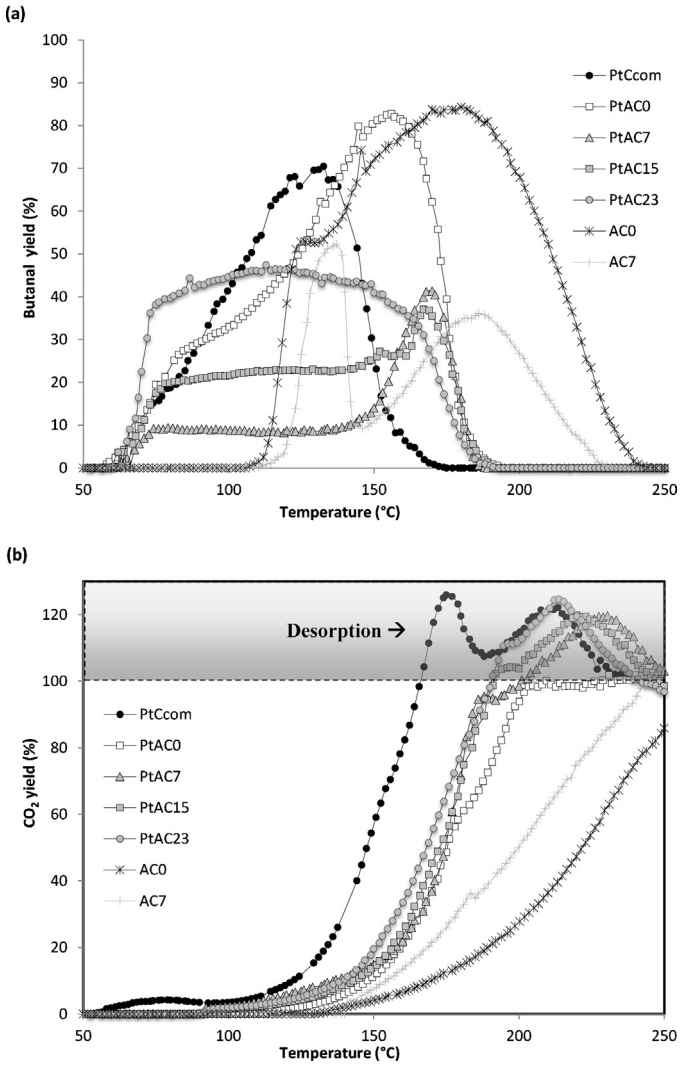

Fig. 6. Butanal (a) and carbon dioxide (b) formation during n-butanol complete oxidation for the used catalysts.

According to this reaction scheme, acetic acid would be formed from butene as already observed in the literature over VO_x-TiO_2 catalysts [47,48]. Slick and DeGroot have demonstrated that the sites that are supposed to be responsible of this reaction are the reducible sites of VO_x-TiO_2 catalysts [49] and such reducible sites can also be found in ceria material. Methanol is formed from acetic acid using the reducible Lewis acid sites (Ce_s^{4+}) and the reactive Lewis base sites (O_s^{2-}) of ceria. These sites are also responsible for the formation of acetone from acetic acid as reported in the literature [50]. A simultaneous dehydrogenation and decarboxylation of butyric acid formed from butanal can be drawn leading to propene. This propene formation occurs using the Lewis acid and base sites of ceria (Ce_s^{4+} and O_s^{2-}). The hydration of propene leads to the formation of two isomers of propanol. Isopropanol oxidation leads to acetone formation whereas 1-propanol oxidation leads to propanal formation, from which ethanol can be formed.

3.2.2. Acetic acid oxidation

The T_{50} and T_{90} values for acetic acid complete oxidation as well as the selectivity to CO_2 at the corresponding temperatures are summarized in Table 3. Carbon dioxide formation plots are presented in Fig. 9. It can be seen a noticeable effect of addition of ceria to Pt-based catalysts supported on alumina.

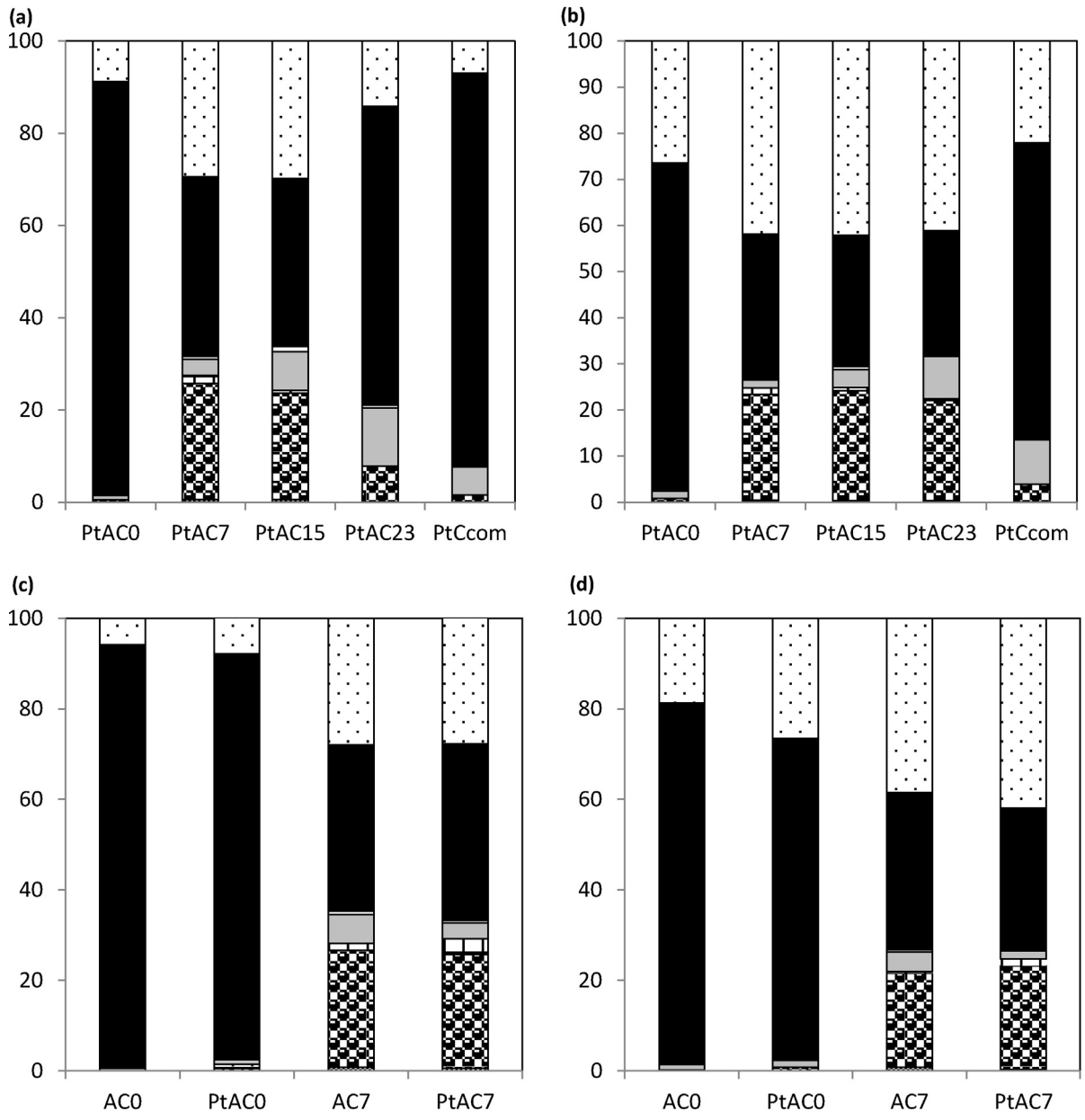

Fig. 7. Selectivity to CO_2 (⊡), butanal (■), acetic acid (□), acetone (▩), ethanol (▣), methanol (▨) and formaldehyde (▩) at T_{50} (a) and (c) and at T_{90} (b) and (d).

In fact an addition of a small amount of ceria (7 wt%) leads to a significant decrease of T_{50} and T_{90} for the complete oxidation of acetic acid. Actually, the temperatures required to obtain conversions of 50 and 90% with the catalyst supported on pure alumina prepared by sol–gel method are 268 and 286 °C respectively while the same conversions are obtained with the Pt-catalyst containing 7 wt% of ceria at 223 and 242 °C respectively. This promoting effect increases with the higher ceria loading (Table 3).

Table 3
T_{50} and T_{90} values of platinum catalysts used for acetic acid oxidation.

	Acetic acid oxidation		Selectivity to CO_2 (%)	
Catalysts	T_{50} (°C)	T_{90}(°C)	at T_{50}	at T_{90}
AC_0	298	307	96	97
AC_{51}	216	226	80	87
PtC_{com}	185	204	86	91
$PtAC_0$	268	286	94	95
$PtAC_7$	223	242	89	93
$PtAC_{15}$	209	223	83	89
$PtAC_{23}$	209	221	87	91
$PtAC_{51}$	201	215	91	95

As shown in Table 3, acetic acid oxidation is not 100% selective to CO_2. Acetone, methanol and formaldehyde are the main intermediate products observed during this reaction. $PtAC_0$ is the most selective to CO_2 at T_{50} and T_{90} (Table 3). Addition of ceria to alumina decreases the selectivity to CO_2 by promoting the formation of the intermediate products as shown for n-butanol oxidation whereas addition of platinum increases the selectivity to CO_2. Indeed, addition of 50% of ceria lowers the selectivity to CO_2 by 10% and the addition of platinum to AC_{51} increases the selectivity to CO_2 from 80 to 91% at T_{50} and from 87 to 95% at T_{90}.

Nevertheless, regardless of the preparation method, the catalysts supported on the mixed oxide CeO_2–Al_2O_3 exhibit better catalytic activity than those supported on pure alumina. To understand these catalysts behaviors previous works related to the redox and acid–base properties of CeO_2–Al_2O_3 oxides should be

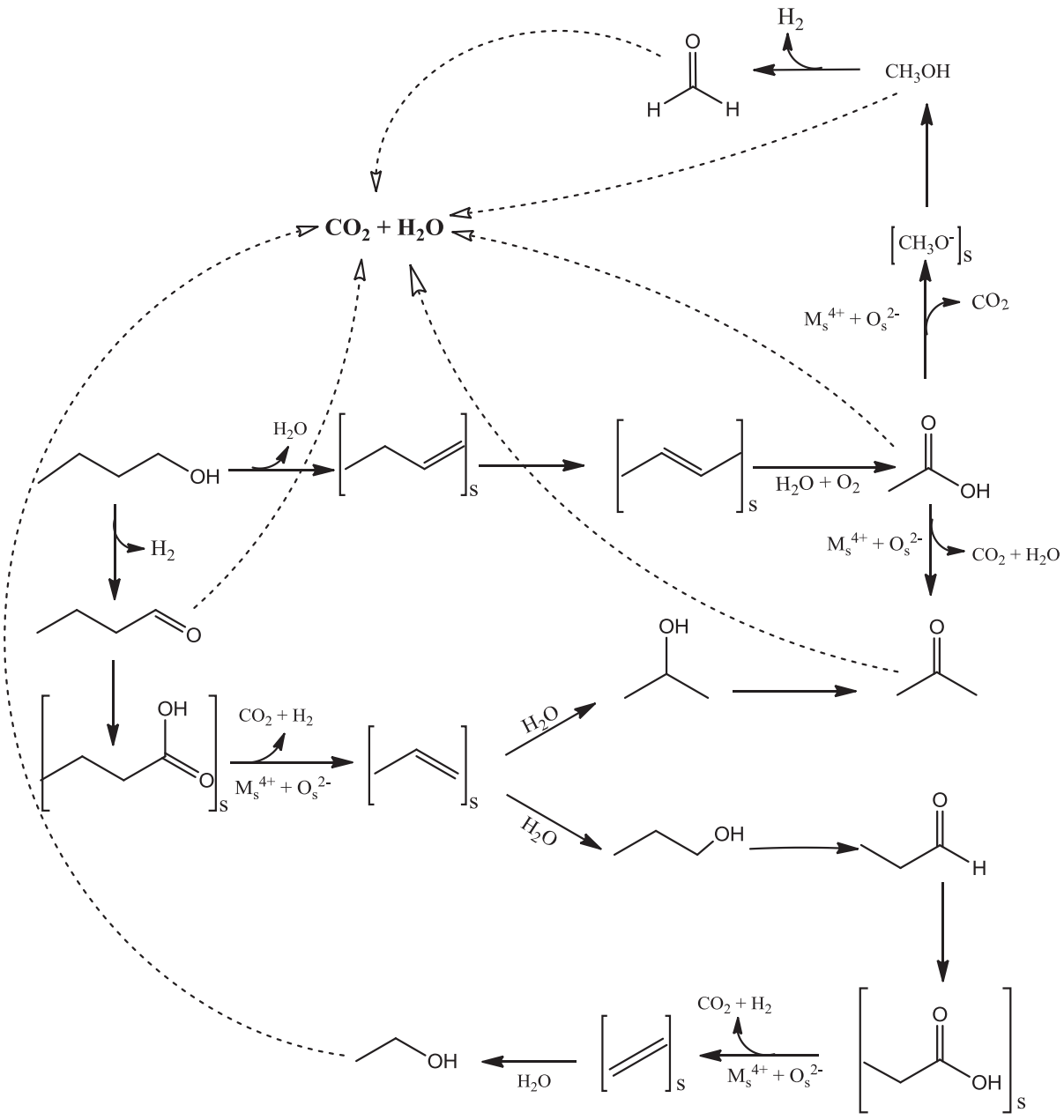

Fig. 8. Reaction pathways of by-products and products formation during n-butanol oxidation.

considered. Indeed, the enhancement of the oxygen storage capacity has been claimed as one of the main responsible for such an effect [51]. This enhancement is due to the particular ability of ceria to undergo deep and rapid reduction/oxidation cycles according to the reaction: $CeO_2 \leftrightarrow CeO_{2-y} + y/2\, O_2$ $(0 \leq y \leq 0.5)$ upon interaction with reducing and oxidizing agents present in the reaction conditions. The role of metal/ceria interface should be also taken into account since TPR analyses and OSC measurements have shown the lowering of the temperature of ceria reduction (Fig. 4), and the enhancement of the oxygen storage capacity (Fig. 5) in presence of platinum.

In order to evaluate the involvement of metal/ceria interaction in this reaction the activities of two carriers (AC_0 and AC_{51}) have been also compared (Fig. 9). It appears that the mixed oxide AC_{51} is more active than pure alumina, $PtAC_0$ and $PtAC_7$. In Table 3 it can be seen that the temperature required to obtain an acetic acid conversion of 50 or 90% is lowered by about 80 or 20 °C when the material used is AC_{51} or $PtAC_0$ respectively instead of AC_0. This result shows the important promoting effect of ceria compared to that of addition of a small amount of platinum and it is in accordance with the OSC measurements (Fig. 5). Indeed the OSC value of AC_{51} (226 μmol O/g) is higher than those of AC_0 (0 μmol O/g), $PtAC_0$ (8 μmol O/g) and $PtAC_7$ (122 μmol O/g).

Since the mechanism of the acetic acid oxidation begins probably with the adsorption of gaseous acetic acid on an acid site of the support followed by abstraction of the acid proton of acetic acid by a basic site [50], the acid–base properties of the support can also affect the catalytic activity. In fact Martin and Duprez have reported that the presence of ceria on alumina decreases its acidity and increases its basicity [52]. Considering the abstraction of the acid proton of acetic acid as the limiting step, the presence of an excess of oxygen species at the ceria surface could be expected to

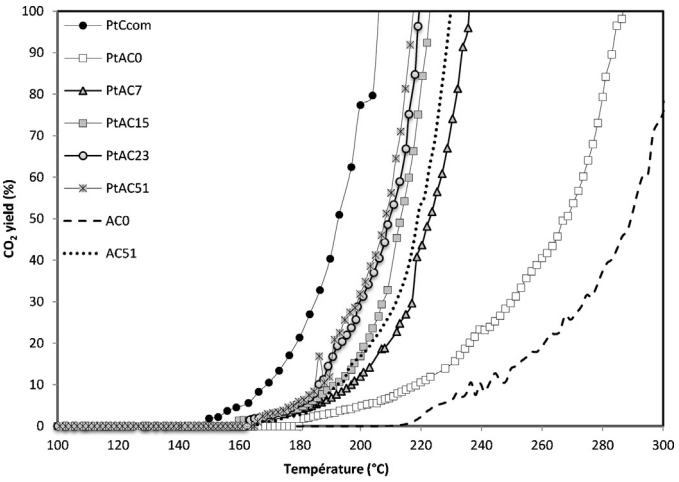

Fig. 9. Carbon dioxide formation on Pt based catalysts, AC_0 and AC_{51} for the oxidation of acetic acid.

favor the decomposition of acetic acid by contributing to form and decompose acetate surface species following the reaction proposed by Hasan *et al.* [50]:

$$CH_3COOH + [Ce^{4+} + O^{2-}]_s \rightarrow [CH_3COO^- + Ce^{4+}]_s + [OH^-]_s$$
$$\rightarrow [CH_3O^-]_s + [H\text{-}Ce^{3+}]_s + CO_2.$$

Thus, the basic nature of ceria, coupled to its redox properties, contributes to the effectiveness of the catalysts.

4. Conclusion

The addition of ceria to alumina leads to the modifications in the physical and chemical properties of the material. In fact morphology measurements show a decrease of the material specific surface area with the addition of ceria. TPR results reveal that the presence of ceria affects the reducibility of the material surface. This result is in accordance with those of OSC measurements which show an increase of the oxygen storage capacity when increasing the ceria loading.

Even if the addition of ceria to platinum based alumina catalysts does not show an important effect on n-butanol oxidation, the catalytic activity is enhanced for acetic acid destruction. This result clearly shows the influence of the VOC nature on the effect of ceria. Nevertheless, in all cases acetic acid is more difficult to oxidize than n-butanol.

The addition of ceria to platinum based alumina catalysts leads to the formation of numerous intermediates products. The role of the metal in the formation of these intermediates products is found to be minor compared to that of ceria. Thus in the reaction pathway proposed to explain the formation of these products, only the active sites of ceria are considered.

References

[1] H.-M. Liang, C.-M. Liao, Chemosphere 68 (2007) 781–789.
[2] L. Malherbe, C. Mandin, Atmospheric Environment 41 (2007) 6322–6330.
[3] K. Pirkanniemi, M. Sillanpää, Chemosphere 48 (2002) 1047–1060.
[4] P. Le Cloirec, Lavoisier Eds, Paris, (1998).
[5] A.C. Gluhoi, B.E. Nieuwenhuys, Catalysis Today 119 (2007) 305–310.
[6] S. Ojala, S. Pitkäaho, T. Laitinen, N.N. Koivikko, R. Brahmi, J. Gaálová, L. Matejova, A. Kucherov, S. Päivärinta, C. Hirschmann, T. Nevanperä, M. Riihimäki, M. Pirilä, R.L. Keiski, Topics in Catalysis 54 (2011) 1224–1256.
[7] J. Hermia, S. Vigneron, Catalysis Today 17 (1993) 349–358.
[8] M.A. Palazzolo, B.A. Tichenor, Environmental Progress 6 (1987) 172–176.
[9] P. Papaefthimiou, T. Ioannides, X.E. Verykios, Applied Catalysis B: Environmental 13 (1997) 175–184.
[10] A. Janbey, W. Clark, E. Noordally, S. Grimes, S. Tahir, Chemosphere 52 (2003) 1041–1046.
[11] P. Papaefthimiou, T. Ioannides, X.E. Verykios, Catalysis Today 54 (1999) 81–92.
[12] L.F. Liotta, Applied Catalysis B: Environmental 100 (2010) 403–412.
[13] P. Marécot, A. Fakche, B. Kellali, G. Mabilon, P. Prigent, J. Barbier, Applied Catalysis B: Environmental 3 (1994) 283–294.
[14] C.-H. Wang, S.-S. Lin, Applied Catalysis A: General 268 (2004) 227–233.
[15] D. Delimaris, T. Ioannides, Applied Catalysis B: Environmental 89 (2009) 295–302.
[16] R.D. Gonzalez, M. Nagaia, Applied Catalysis 18 (1985) 57–70.
[17] P. Papaefthimiou, T. Ioannides, X. Verykios, Applied Thermal Engineering 18 (1998) 1005–1012.
[18] H. Shinjoh, H. Muraki, Y. Fujitani, Applied Catalysis 49 (1989) 195–204.
[19] K.T. Chuang, B. Zhou, S. Tong, Industrial and Engineering Chemistry Research 33 (1994) 1680–1686.
[20] J. Chi-Sheng Wu, T.-Y. Chang, Catalysis Today 44 (1998) 111–118.
[21] A. Trovarelli, Catal. Rev.-Sci. Eng. 38 (1996) 439–520.
[22] J.C. Summers, S.A. Ausen, Journal of Catalysis 58 (1979) 131–143.
[23] S. Damyanova, J.M. Bueno, Applied Catalysis A: General 253 (2003) 135–150.
[24] D. Andreeva, R. Nedyalkova, L. Ilieva, M. Abrashev, Applied Catalysis A: General 246 (2003) 29–38.
[25] R. Ramírez-López, I. Elizalde-Martinez, L. Balderas-Tapia, Catalysis Today 150 (2010) 358–362.
[26] X.-S. Huang, H. Sun, L.-C. Wang, Y.-M. Liu, K.-N. Fan, Y. Cao, Applied Catalysis B: Environmental 90 (2009) 224–232.
[27] P. Djinović, J. Levec, A. Pintar, Catalysis Today 138 (2008) 222–227.
[28] Z. Abbasi, M. Haghighi, E. Fatehifar, S. Saedy, Journal of Hazardous Materials 186 (2011) 1445–1454.
[29] S.H. Oh, P.J. Mitchell, R.M. Siewert, Journal of Catalysis 132 (1991) 287–301.
[30] I. Maupin, J. Mijoin, J. Barbier Jr., N. Bion, T. Belin, P. Magnoux, Catalysis Today 176 (2011) 103–109.
[31] L. Kai, W. Xuezhong, Z. Zexing, W. Xiaodong, W. Duan, Journal of Rare Earths 25 (2007) 6–10.
[32] L. Oliviero, J. Barbier Jr., D. Duprez, H. Wahyu, J.W. Ponton, I.S. Metcalfe, D. Mantzavinos, Applied Catalysis B: Environmental 35 (2001) 1–12.
[33] H.R. Devlin, I.J. Harris, Industrial and Engineering Chemistry Fundamentals 23 (1984) 387–392.
[34] J. Mikulová, S. Rossignol, J. Barbier Jr., D. Duprez, C. Kappenstein, Catalysis Today 124 (2007) 185–190.
[35] J. Mikulová, J. Barbier Jr., S. Rossignol, D. Mesnard, D. Duprez, C. Kappenstein, Journal of Catalysis 251 (2007) 172–181.
[36] A.A. Klinghoffer, R.L. Cerro, M.A. Abraham, Catalysis Today 40 (1998) 59–71.
[37] N. Ali, C. Lu, R. Masel, Catalysis Today 62 (2000) 347–353.
[38] J. Fonseca, S., Royer, N., Bion, L. Pirault-Roy, M. do C. Rangel, D., Duprez, F., Epron, Applied Catalysis B: Environmental.
[39] D. Duprez, Journal de Chimie Physique et de Physico-Chimie 80 (1983) 487–505.
[40] S. Kacimi, J. Barbier, R. Taha, D. Duprez, Catalysis Letters 22 (1993) 343–350.
[41] S. Rossignol, Y. Madier, D. Duprez, Catalysis Today 50 (1999) 261–270.
[42] J.Z. Shyu, K. Otto, Journal of Catalysis 115 (1989) 16–23.
[43] Y.I. Yermakov, B.N. Kuznetsov, Journal of Molecular Catalysis 9 (1980) 13–40.
[44] A.C.S.F. Santos, S. Damyanova, G.N.R. Teixeira, L.V. Mattos, F.B. Noronha, F.B. Passos, J.M.C. Bueno, Applied Catalysis A: General 290 (2005) 123–132.
[45] H.C. Yao, Y.F.Y. Yao, Journal of Catalysis 86 (1984) 254–265.
[46] B. Li, S. Li, Y. Wang, N. Li, W. Zhang, B. Lin, Chinese Journal of Catalysis 31 (2010) 528–534.
[47] W.Y. Suprun, D.P. Sabde, H.-K. Schädlich, B. Kubias, H. Papp, Applied Catalysis A: General 289 (2005) 66–73.
[48] W. Suprun, E.M. Sadovskaya, C. Rüdinger, H.-J. Eberle, M. Lutecki, H. Papp, Applied Catalysis A: General 391 (2011) 125–136.
[49] W.E. Slink, P.B. DeGroot, Journal of Catalysis 68 (1981) 423–432.
[50] M.A. Hasan, M.I. Zaki, L. Pasupulety, Applied Catalysis A: General 243 (2003) 81–92.
[51] M. Centeno, M. Paulis, M. Montes, J. Odriozola, Applied Catalysis A: General 234 (2002) 65–78.
[52] D. Martin, D. Duprez, Journal of Molecular Catalysis A: Chemical 118 (1997) 113–128.